Two-dimensional turbulence analysis using high-speed visible imaging in TJ-II edge plasmas.

J.A. Alonso*, S.J. Zweben[1], J.L. de Pablos, E. de la Cal, C. Hidalgo,
T. Klinger[2], B.Ph. van Milligen, M.A. Pedrosa, C. Silva[3], H. Thomsen[2]
Laboratorio Nacional de Fusión, Asociación EURATOM-CIEMAT, 28040 Madrid, Spain
[1] Princeton Plasma Physics Laboratory, Princeton, NJ, USA
[2] Max-Planck-Institut für Plasma Physik, EURATOM Ass., 17491 Greifswald, Germany
[3] Associação Euratom/IST, Centro de Fusão Nuclear, Instituto Superior Técnico

Abstract

Two-dimensional edge plasma turbulence as measured by high-speed H_α imaging is investigated in the TJ-II stellarator. An image analysis method based on two-dimensional continuous wavelet transformation (2D-CWT) is introduced. This method detects localized coherent structures (blobs) in the images and extracts their geometrical characteristics (position, scale, orientation angle and aspect ratio). We study the impact of edge shear-layers (both spontaneous and biased-induced) on these geometrical aspects of blobs. Results show a reduction in the angular dispersion of $k \sim 1.2 - 1.4$ cm^{-1} blobs as the shear layer (both spontaneous and biased-induced) is established in the boundary, as well as a shift of the aspect ratio histogram toward higher values. The turbulence suppression induced by the biasing seems to be scale-selective, more effectively suppressing $k \sim 1.4$ cm^{-1}, $\lambda \sim 0.7$ cm structures than $k \sim 0.7$ cm^{-1}, $\lambda \sim 1.4$ cm ones.

1 Introduction

Transport in fusion devices is a phenomenon with high degree of complexity. Localized layers where $E \times B$ shear stabilization mechanisms are likely playing a role, have extensively been proved to have a beneficial impact in confinement. A reduction in turbulence amplitude is expected and measured [1]. However few attempts have been made to study the effects of such layer on the morphology of turbulent structures [2]. Two-dimensional images of edge plasma turbulence have been obtained by high-speed imaging in the visible range in the edge of tokamak devices [3], [4]. This paper reports a 2-D visualization of transport in the plasma edge of TJ-II stellarator. A wavelet-based image analysis method is used to localize and characterize

*e-mail:ja.alonso@ciemat.es

blob-like structures. The impact of shear flow and external biasing on turbulent structures is investigated by means of this method.

2 Experimental description

Experiments were carried out in TJ-II plasmas Electron Cyclotron Resonance heated (P_{ECRH}= 200 - 400 kW, B_T = 1 T, R = 1.5 m, $\langle a \rangle$ = 0.22 m, $\frac{\iota(a)}{2\pi} \approx$1.6).

For the 2D turbulence studies presented here two different cameras were used. First model is a Princeton Scientific Instruments intensified camera with CCD sensor (PSI-5), achieving recording rates up to 250.000 frames per second. The storage capacity is 300 frames with 64 by 64 pixels resolution, thus giving 1.2ms total recording time at maximum speed with an image every 4μs. Second is a Phantom v7.1 by Photo-sonics International LTD, with CMOS sensor. Recording speed is 120.000 fps with 64 by 64 frame resolution. Recording durations can be of hundreds of milliseconds.

Both cameras were placed in an optical bench one meter away from TJ-II stellarator central coil for them not to be affected by the prompt rise/fall of magnetic fields. The image was taken from the port to the camera sensor by means of a coherent fiber bundle and a suitable set of lenses. A H_α filter is placed in the front lens.

Neutral recycling at the poloidal limiter is used to light up the outer plasma region ($\rho \sim$-1). The view plane is in a near-poloidal cross-section with optimized B-field perpendicularity (see Fig.1).

Bright structures are frequently seen with a spatial extent of few centimeters. Those structures show predominant poloidal movements with typical speeds of 10^3 - 10^4 ms^{-1} in agreement with the expected $\mathbf{E} \times \mathbf{B}$ drift rotation direction. Moreover, projection of the magnetic field lines on the image frame, reveals little or no velocity component in the field line direction . It should be noticed that, with this light cloud thickness, long parallel structures can have a parallel velocity component not visible from the camera position.

3 Image processing with 2-D directional continuous wavelets

Image analysis techniques were implemented for detecting blobs and characterising their geometry (aspect ratio, orientation...). As ‘blobs’ we mean the localized coherent structures seen in the images. A Two-dimensional continuous wavelet transformation (2D-CWT) was found to be suitable for these purposes. A thorough introduction to the 2D-CWT can be found in [5]. We outline here only the necessary formalism to make the following explanation clear. The transformation is given by:

$$S(a,\vec{b}) = \langle \psi_{a,\vec{b}}(\vec{x}) | f(\vec{x}) \rangle \ ,$$

where $\psi(\vec{x})$ is the analysing wavelet and $\psi_{a,\vec{b}}(\vec{x}) = \frac{1}{a}\psi\left(\frac{\vec{x}-\vec{b}}{a}\right)$, whereas $f(\vec{x})$ is the image function. Angle brackets stands for spatial integration. In the two dimensional case, anisotropic wavelets can be constructed, the transformation being labeled with an additional angle parameter θ, $\psi_{a,\vec{b},\theta}(\vec{x}) = \frac{1}{a}\psi\left(\frac{r_{-\theta}(\vec{x}-\vec{b})}{a}\right)$, where $r_{-\theta}$ is the θ-rotation matrix. This allows the extraction of oriented features.

The method presented here has a detection-recognition scheme based on isotropic (detection) and anisotropic (recognition) 2D-CWT [6].

In a first stage blobs are localised. The image is wavelet-transformed with a Mexican hat wavelet,

$$\psi^{MexHat}(x,y) = (2-x^2-y^2)e^{-\frac{x^2+y^2}{2}} \ .$$

The result contains original image structures with a scale comparable to that of the analysing wavelet. Weak structures are removed after thresholding. The threshold is chosen higher for smaller scales which are more affected by noise. Local extrema (both positive and negative) are regarded as blob positions $\vec{b}_j,\ j = 1..N_{blobs}$.

The Mexican hat wavelet fourier spectrum has a mean wave vector $\hat{k} = \frac{2\sqrt{2}}{\sqrt{\pi}}$ and $\sigma_k = \sqrt{3-\frac{8}{\pi}}$, which transform inversely with the scale parameter a. Considering this and the image resolution, three scales were used in the analysis, say $\left[1, \frac{1}{2}, \frac{1}{4}\right]$.

At a second stage the Morlet wavelet,

$$\psi^{Morlet}(x,y) = \left(\cos(k_0 y) - e^{-\frac{1}{2}k_0^2}\right) e^{-\frac{1}{2}(\varepsilon^{-1}x^2+y^2)} \ , \tag{1}$$

was used for directional analysis. The choice of wave vector k_0 and anisotropy parameter ε is a compromise between different requirements. On the one hand, angular resolving power is an increasing function of both k_0 and ε [5]. On the other hand, spatial locality (increasing with decreasing ε) as well as scale matching with the Mexican hat (which affects k_0) are necessary. Our choice was $k_0 = 3$, $\varepsilon = 1$ and it was introduced an offset scale $a_0 = 1.875$ for scale correspondence with Mexican hat wavelet.

Angular convolution with the Morlet wavelet gives the angular response curve of the j-th blob detected $W^{(j)}(\theta) = \langle \psi^{Morlet}_{a,\vec{b}_j,\theta}(\vec{x}) | f(\vec{x}) \rangle$. From this curve, a blob's orientation angle $\hat{\theta}$ can be inferred. $\hat{\theta}$ is the angle between blob's principal axis (direction of blob's maximum extent) and the frame x-axis (see Fig.3). No precise mapping of magnetic surfaces over the images was yet made, so that scales and angles presented here are not referred to local magnetic coordinates (i.e. radial-poloidal coordinates) but to frame coordinates.

The aspect ratio (the ratio of blob dimension along its principal axis to the dimension along an axis perpendicular to this) can be estimated as $AR^{(j)} = \sqrt{\frac{W^{(j)}(\hat{\theta})}{W^{(j)}(\hat{\theta}+\pi/2)}}$.

4 Impact of edge shear-layer in 2D turbulence structure

A naturally occurring shear-layer has been observed in TJ-II edge plasmas [7, 8] which is self-organized near marginal stability with fluctuations, . It is formed in certain magnetic configurations above a density threshold ($\sim 0.6 \times 10^{19} \mathrm{m}^{-3}$), though its appearance is linked with several magnetic and plasma parameters [8]. The controllable occurrence of this shear-layer allows us to study its impact on turbulent structures.

Several image sequences for shots with and without shear-layer were analysed. Frame size in this series of shots was 11 cm $\times$ 11 cm.

For a blob to be considered orientable its aspect ratio must exceed a chosen value (2 in the presented results). The percent of blobs exceeding that value is the percentage of elongated blobs (fifth column) which is a measure of the shift of the aspect ratio histogram toward higher values. Finally, $\hat{\Theta}$ and σ_Θ stand as the mean angle of those elongated blobs and the standard deviation of their angular distribution. This standard deviation is an indication of the level of order of the blob population. Large STDs mean that blobs are randomly oriented, whereas small values mean that blobs point in roughly the same direction.

In order to avoid edge effects in determining blob characteristic parameters, only frame-centered blobs were included in the statistics.

Fig4.a shows the standard deviation of the so-obtained angular distribution of turbulent structures against density. Each point correspond to a 300-frames series acquired in different shots. A clear reduction of angular dispersion is observed as density rises and shear layer is developed.

Fig4.b shows the density dependence of the percentage '% of elongated blobs'. A slight though perceptible positive dependence on line averaged density can be noticed in this plot.

Mean H_α profiles were measured for these shots. For increasing densities, images shows higher Hα emission but no reduction of the light cloud, which might be affecting our data interpretation, was observed.

5 Turbulence structure modification during external biasing induced improved confinement regime.

Improved confinement regimes are accessible in TJ-II stellarator through external biasing [9]. Plasma edge is biased with graphite electrode installed in a fast reciprocating probe drive. The electrode was inserted typically 2 cm inside the LCFS and biased with respect to one of the two TJ-II limiters [10].

The long recording capabilities of Phantom v7.1 fast camera allowed us to study the biasing turning-off from improved to normal regime. A 17 ms long shot with 19 cm $\times$ 19 cm frame

size was analysed. First results confirm the deep impact of external biasing in plasma edge structures.

Figure 5 shows the electron density to H_α ratio evolution evidencing the better confinement during biasing (5.a). The frame RMS (calculated as the square root of the sum to every pixel of the squared pixel intensity) reflects the relative increase in turbulence activity (5.b). The number of turbulent structures detected at all three different scales also increases when biasing is turned off (5.c-e) again reflecting an increase in turbulent activity. However, the increase is not the same for all the analysed scales, being particularly intense for the intermediate scale ($k \sim 1.4$ cm^{-1}). It can be seen that ratio of medium scale ($k \sim 1.4$ cm^{-1}) to big scale ($k \sim 0.7$ cm^{-1}) blob population changes from 0.4 during biasing to 0.8 after biasing.

It must be emphasized that number of blobs per frame in each scale is not to be taken as an absolute value since smaller scales are more affected by noise and therefore the threshold for detection has to be more severe. However this change in relative scale activity is a meaningful modification of turbulence structure.

The effect of biasing on turbulent structures was also noticeable in the standard deviation of angular distribution (for the $k \sim 1.4$ cm^{-1} structures, it changes from 18deg during biasing to 29deg after it) as well as in the percentage of elongated blobs (from 47% to 34% for the $k \sim 1.4$ cm^{-1}). Similar tendency was found in the blobs with $k \sim 0.7$ cm^{-1}. Not enough $k \sim 2.8$ cm^{-1} structures were detected for significant statistics.

Figure 6 is an example of the structure detection applied to one frame during biasing (upper left image) and after biasing (lower left image). The continuous wavelet transform in three different scales extracts structures around wavelet scale: $k \sim 0.7$ cm^{-1} structures in second column, $k \sim 1.4$ cm^{-1} in third column and $k \sim 2.8$ cm^{-1} in fourth column. It can be seen the relative increase in medium scale structures from the frame before biasing turning-off (top) to the frame after biasing (bottom).

6 Conclusions

Two dimensional plasma edge turbulence was investigated by means of fast imaging in the visible range. A continuous wavelet-based method was used to localize and study the geometry of coherent turbulent structures (scale, aspect ratio and orientation angle) in different plasma regimes.

Firstly the impact of the naturally occurring shear-layer, self-organized near marginal stability, on TJ-II edge turbulent structures was addressed.

Experimental results show a reduction in the angular dispersion of $k \sim 1.2$ cm^{-1} blobs as the shear layer is established in the boundary, as well as a slight though sensible shift of the aspect

ratio histogram toward higher values (fig.4). These results are consistent with the picture of the shear layer stressing blobs as well as ordering them. Neither significant changes in turbulence intensity (as the number of blobs detected) nor a clear reduction in turbulence scale could be detected with present fast camera experimental setup and analyzing method. It should be noted that spontaneous edge sheared flow and fluctuations are near marginal stability. However, probe measurements show that when sheared flow are developed the level of fluctuations decreases [8].

Secondly it was studied the effect of external biasing on the blob relative populations of the three different scales analysed ($k \sim 0.7$ cm^{-1}, 1.4 cm^{-1}, 2.8 cm^{-1}).

An increase in all the analysed scales was observed when biasing is removed. This increase is more noticeable for the intermediate scales $k \sim 1.4$ cm^{-1}. During external biasing the standard deviation of these structures was significantly less than after biassing turn-off and the aspect ratio histogram was relatively shifted toward higher values.

This result shows a deep modification in k power spectrum during external biasing induced improved confinement regimes, not only in its integrated power but also in its shape.

References

[1] P. W. Terry, Rev. Mod. Phys. **72**, 109 (2000).

[2] H. Thomsen *et al*, in *Proc. 32nd EPS conference on Control. Fusion and Plasma Physics* (ECA, Tarragona, 2005), p. P5.027.

[3] S. J. Zweben *et al*, Nucl. Fusion **44**, 134 (2004).

[4] J. L. Terry *et al*, Phys. Plasmas **10**, 1739 (2003).

[5] *Wavelets in Physics*, edited by J. C. van den Berg (Cambridge University Press, Cambridge CB2 2RU, UK, 1999).

[6] J.-P. Antoine, CWI Quarterly **11**, 323 (1998).

[7] C. Hidalgo, M. A. Pedrosa, L. García, and A. Ware, Phys. Rev. E **70**, 1 (2004).

[8] M. A. Pedrosa *et al*, Plasma Phys. Control. Fusion **47**, 777 (2005).

[9] C. Hidalgo *et al*, Plasma Phys. Control. Fusion **46**, 287 (2004).

[10] C. Silva *et al*, in *Proc. 32nd EPS conference on Control. Fusion and Plasma Physics* (ECA, Tarragona, 2005), p. P2.037.

Tables

Shot#	n_e (10^{19}m^{-3})	N_b	Scale Ratio	%Elongated	$\hat{\Theta}$	σ_Θ
12361	1.10	204	0.15	30	46	30
12367	0.76	202	0.07	22	50	29
12369	0.84	188	0.16	30	44	31
12370	1.10	144	0.06	35	42	29
12372	1.20	179	0.21	30	45	29
12378	0.81	171	0.10	23	36	34
12365	0.39	184	0.01	27	127	46
12371	0.43	176	0.03	25	39	42
12373	0.49	212	0.05	26	34	43
12375	0.50	187	0.16	18	38	40
12386	0.47	160	0.06	20	61	32
12387	0.51	136	0.27	19	15	33

Table 1: blob statistics of analysed shots

Figure Captions

Figure 1. View plane and field lines by the poloidal limiter used for plasma edge lightening. Broad lines stand for the toroidal extent of the light cloud.

Figure 2. Time averaged H_α emision. (a)Perpendicular view of the limiter. (b)Profiles along the lines marked in (a).

Figure 3. Principal axis of two structures

Figure 4. Density dependence of the standard deviation of blobs angular distribution (left) and population of elongated blobs (right)

Figure 5. Time evolution of electron density to H_α ratio (a), frame root mean square (b) and 50-frames averaged number of structures per frame in different scales (c-e), during and after biasing (shot#13721).

Figure 6. Structure detection in two frames of shot #13721, during (top) and after biasing (bottom). White pluses indicate detected blobs positions.

Figures

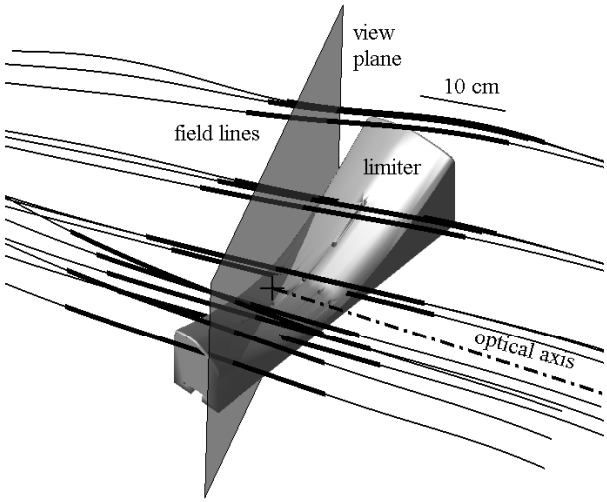

Figure 1: View plane and field lines by the poloidal limiter used for plasma edge lightening. Broad lines stand for the toroidal extent of the light cloud.

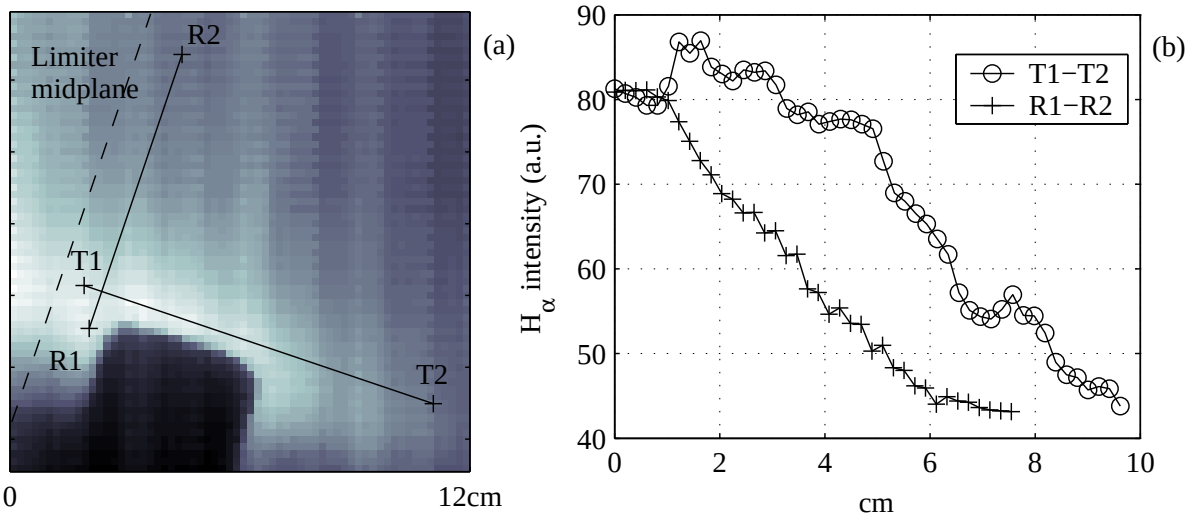

Figure 2: Time averaged H_α emision. (a)Perpendicular view of the limiter. (b)Profiles along the lines marked in (a).

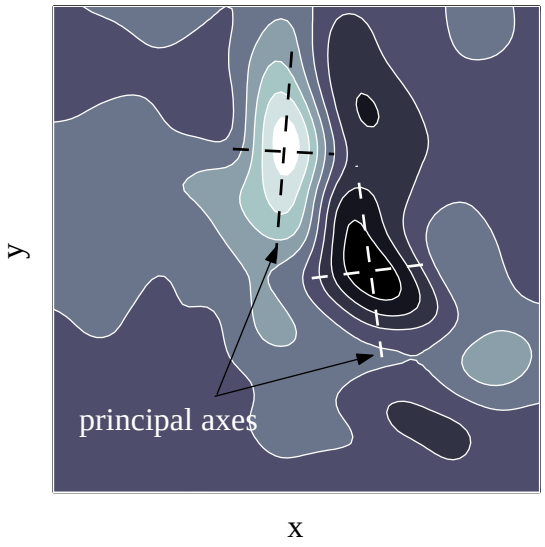

Figure 3: Principal axis of two structures

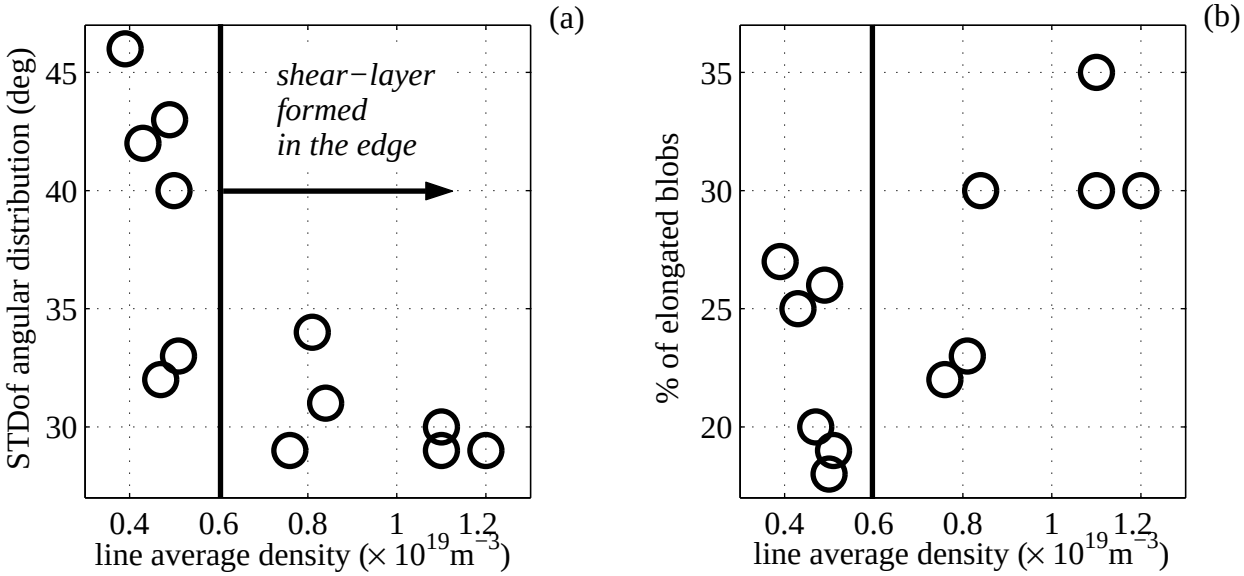

Figure 4: Density dependence of the standard deviation of blobs angular distribution (left) and population of elongated blobs (right)

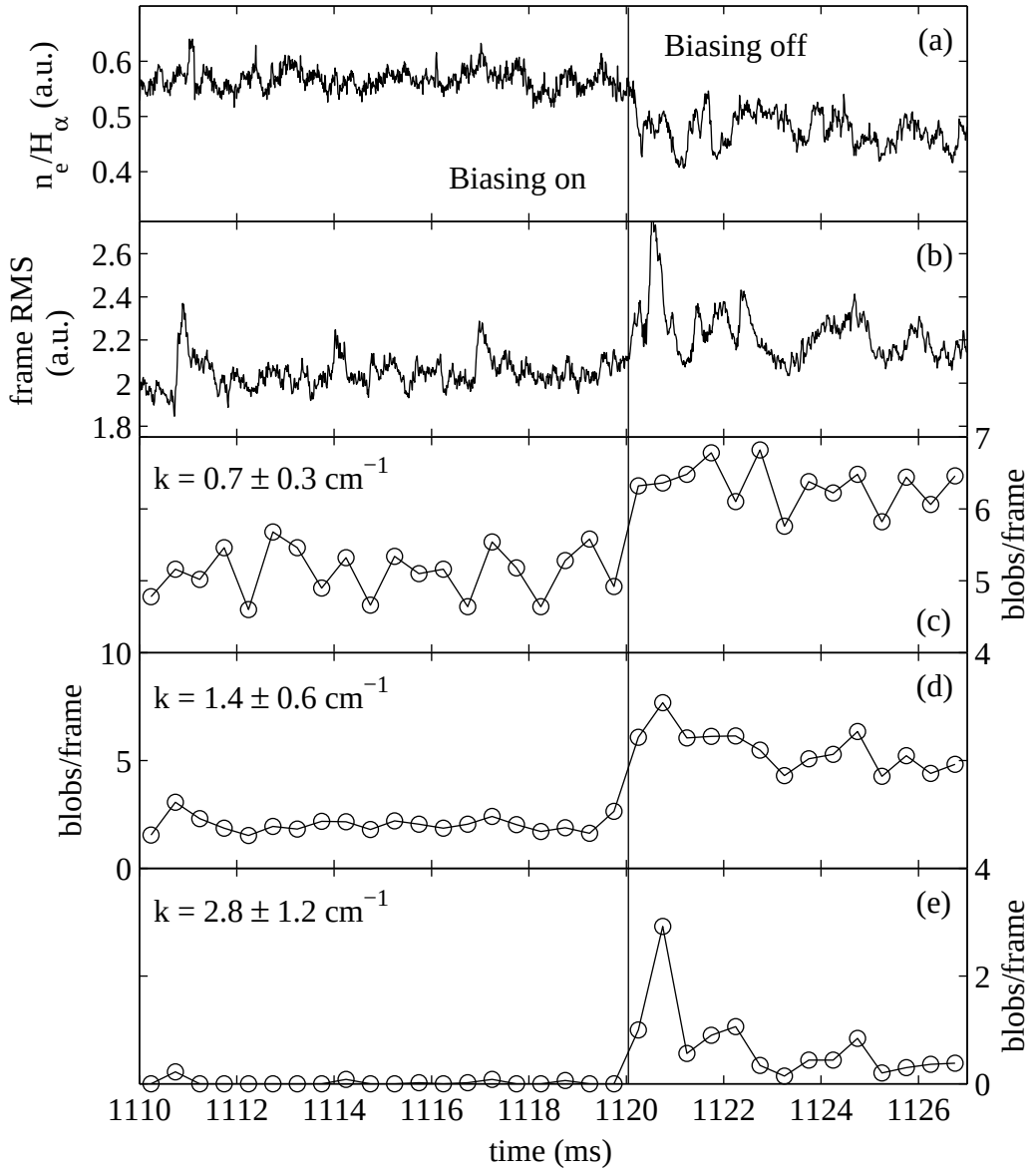

Figure 5: Time evolution of electron density to H_α ratio (a), frame root mean square (b) and 50-frames averaged number of structures per frame in different scales (c-e), during and after biasing (shot#13721).

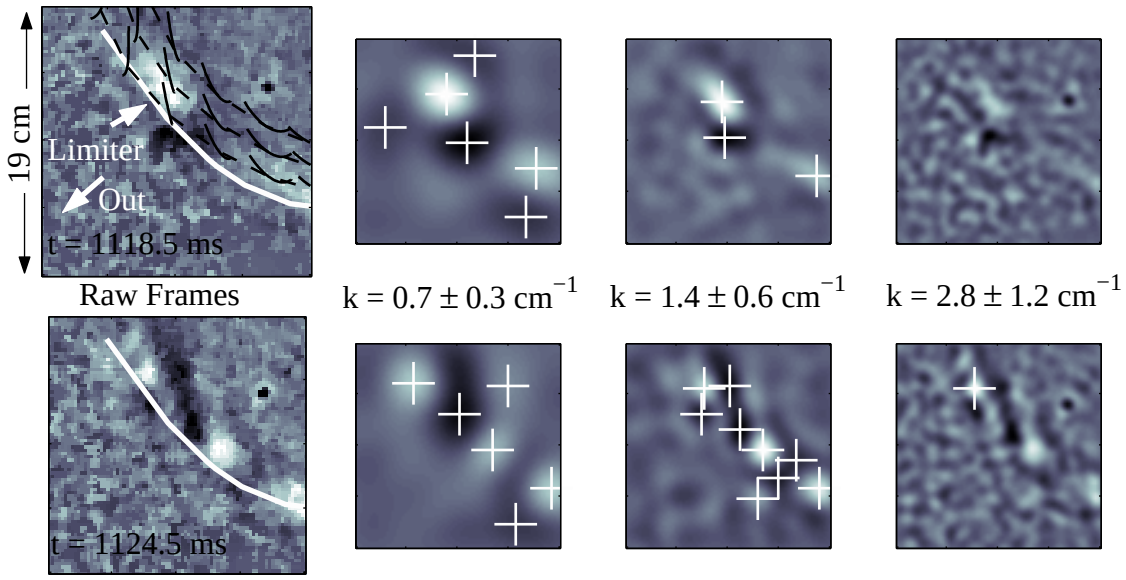

Figure 6: Structure detection in two frames of shot #13721, during (top) and after biasing (bottom). White pluses indicate detected blobs positions.